

# SCIENTIFIC REPORTS



OPEN

## A humanized anti-DLL4 antibody promotes dysfunctional angiogenesis and inhibits breast tumor growth

Received: 02 February 2016

Accepted: 27 May 2016

Published: 15 June 2016

Xuelian Jia<sup>1,\*</sup>, Wenyi Wang<sup>1,2,\*</sup>, Zhuobin Xu<sup>1</sup>, Shijing Wang<sup>1</sup>, Tong Wang<sup>1</sup>, Min Wang<sup>1</sup> & Min Wu<sup>1</sup>

Blockage of Delta-like 4 (DLL4)-directed Notch signaling induces excessive tip cell formation and endothelial proliferation resulting in dysfunctional angiogenesis in tumors. MMGZ01, as a murine anti-human DLL4 monoclonal antibody, specifically binds to human DLL4 and blocks Notch pathway. Here, the structure of MMGZ01 variable fragment (Fv) was established and framework region (FR) residues which supported complementarily determining region (CDR) loop conformation were identified. Important residues interactions were also identified through docking MMGZ01 Fv with antigen epitope in DLL4. To humanize the murine antibody, we modified MMGZ01 Fv through CDR grafting and the reconstructed antibody (H<sub>3</sub>L<sub>2</sub>) maintained similar structure and binding affinity to parental MMGZ01 after back mutation of 12 canonical murine residues in the FRs. Meanwhile, H<sub>3</sub>L<sub>2</sub> promoted human umbilical vein endothelial cell (HUVEC) proliferation through inhibiting DLL4-directed Notch pathway. Moreover, in MDA-MB-231-bearing nude mice, H<sub>3</sub>L<sub>2</sub> induced dysfunctional angiogenesis and tumor cell apoptosis and showed superior anti-tumor activity. In conclusion, H<sub>3</sub>L<sub>2</sub> is an ideal humanized antibody that inhibits tumor growth through targeting DLL4-Notch pathway and has attracting potentials for clinical applications.

The Notch signaling pathway is implicated with cell fate decision, stem cell renewal and differentiation in many postnatal tissues during development<sup>1</sup>. In mammalian, it consists of four receptors (Notch 1–4) and five canonical ligands (Jagged 1, 2 and Delta-like 1, 3, 4). Overexpressed Notch receptors or ligands activates the Notch-mediated tumorigenesis pathway through deregulating in many hematological malignancies and solid tumors<sup>1,2</sup>.

As a key ligand of Notch pathway, delta-like 4 (DLL4) is endothelium-specific with higher expression in tumor vasculature compared to normal tissues<sup>3</sup>. Through regulating the proliferation of tip cells in sprouting vessels, DLL4 directs the generation of functional and organized vasculatures in tumors<sup>4,5</sup>. Further blockage of DLL4 increases immature capillary sprouting and branching due to excessive tip cell formation and endothelial proliferation, but with reduced vessel lumen size. These dysfunctional vasculatures perform poor perfusion, thus increase hypoxia in tumors<sup>6,7</sup>. Many DLL4/Notch inhibitors have been developed with ideal anti-tumor efficiency in pre-clinical models or clinical trials<sup>2,8,9</sup>.

In a previous study, we developed a murine anti-human DLL4 monoclonal antibody with expected anti-angiogenesis and anti-tumor effects<sup>10</sup>. While murine antibody has the advantage of high antigen binding affinity and specificity, the clinical usefulness of such antibody is still limited to the human anti-mouse antibody (HAMA) response<sup>11,12</sup>. Chimeric antibodies which graft variable regions of murine antibodies onto human constant regions are still likely to induce severe immune response<sup>13,14</sup>. Thus, humanization of murine antibody variable regions becomes a prospective alternative. Jones *et al.*<sup>15</sup> firstly grafted complementarily determining regions (CDRs) in heavy and light chain variable regions (VH, VL) of murine antibody B1–8 onto human antibody and generated a CDR grafted antibody, which possessed comparable affinity with B1–8. However, compared to their

<sup>1</sup>State Key Laboratory of Natural Medicines, School of Life Science & Technology, China Pharmaceutical University, Nanjing, Jiangsu 210009, China. <sup>2</sup>The Rutgers Center for Computational and Integrative Biology, Rutgers University, Camden, NJ 08102, United States. \*These authors contributed equally to this work. Correspondence and requests for materials should be addressed to M.Wang (email: minwang@cpu.edu.cn) or M.Wu (email: mickeywu2001@163.com)

Regions	Templates (PDB ID)	Identity or Similarity (%)	Structure score
LFRs	1E6O. L	87.0	94.6
L-CDR1	3LS5. L	89.7	91.9
L-CDR2	2BRR. X	88.8	95.8
L-CDR3	4ETQ. B	83.7	94.4
HFRs	1E6O. H	89.2	94.7
H-CDR1	1IQW. H	82.3	79.1
H-CDR2	3CMO. Y	83.2	70.2
H-CDR3	3UPC. F	45.6	56.4

**Table 1. Structure templates for MMGZ01 Fv homology modeling.** The overall backbone integrity of each antibody subdomain was assessed by the Structure score, below 50 of which indicates possibilities of structural issues.

parental mouse antibodies, many CDR grafted antibodies present lower antigen binding affinities due to the lack of framework regions (FRs) canonical residues which supported CDR loop conformation<sup>16</sup>.

In this study, we firstly chose suitable human V and J donors for CDR grafting based on a precisely modeled MMGZ01 variable fragment (Fv) structure. Through back mutation of 7 canonical residues in VH and 5 canonical residues in VL to the original murine one, the further designed version (H<sub>3</sub>L<sub>2</sub>) achieved comparable DLL4 binding affinity and specificity with the murine-human chimeric antibody (H<sub>C</sub>L<sub>C</sub>). Comprehensive *in vivo* and *in vitro* evaluation revealed that H<sub>3</sub>L<sub>2</sub> was able to inhibit tumor growth and disturb tumor angiogenesis.

## Results

**Antibody modeling and evaluation.** The amino acid sequences of MMGZ01 VH, VL were loaded to Molecular Operating Environment (MOE) software, version 2013.08, and FRs or CDRs in VH and VL were identified by Kabat numbering scheme<sup>17</sup>. Antibody structures in Protein Data Bank (PDB)<sup>18</sup> were searched and scored based on sequence similarity as well as structural fitness, in particular the backbone integrity, which was evaluated based on a structural scoring scheme developed by MOE. The first task in antibody modeling is to find FRs templates for VH and VL, where, the best scored FRs templates are normally from different antibodies. We comprehensively selected FRs templates from a single antibody 1E6O (see Table 1), in order to get a Fv dimer framework with suitable VH-VL orientation.

As templates for the VH-VL framework were determined, the CDR loops templates were further assigned based on loop length and similarity prior to the grafting of CDRs onto the F<sub>V</sub> dimer framework. In loop grafting, multiple templates were combined, aligned and superposed at the backbone atoms of corresponding residues in the FRs. The CDR residues of CDR templates were bonded to the FRs template and redundant residues were deleted. Four rounds of tethered energy minimization were then applied to relieve strained geometry and atom clashes in the newly composed antibody subdomain. With these steps, a precise structure of MMGZ01Fv was built automatically by MOE Antibody Builder module (Fig. 1a).

A Ramachandran plot was displayed to check the stereo-chemical quality of established Fv structure<sup>19</sup>. Residues were rendered in green if they located in the core region, yellow if in the allowed region and red if in the outlier region. As shown in Fig. 1b, all the residues distributed in the allowed regions, indicating that the established Fv structure is reasonable.

**Epitope mapping.** To identify the epitopes recognized by MMGZ01 and to minimize the possible poses during antibody-antigen docking, a dodecapeptide phage display library was screened<sup>20</sup>. Phage-peptides bound to MMGZ01 were panned and enriched for 4 cycles, followed by monoclonal Enzyme-linked immunosorbent assay (ELISA). The phage clones gave ELISA signal 3-fold of control (3% Bull Serum Albumin, BSA) were DNA sequenced and aligned for consensus motif. As shown in Supplementary Fig. S1, the consensus residues between positive clones were KK—HF-H. These residues were found in DLL4 (residues 189–197) and were likely to constitute a conformational epitope.

**Complex structure of MMGZ01-DLL4 predicted by molecular docking.** Structure model of DLL4 (residue range from 27 to 283) was provided by SWISSMODEL, based on template structure in PDB (PDB ID 4x1wB, sequence identity 80%). Before docking, the epitope residues mapped by phage display library screening were selected as contact residues in DLL4. A rigid receptor docking program ZDOCK<sup>21,22</sup> was used, and the output files gave top 10 modeled prediction of complex structure. The top one complex structure was shown in Fig. 1c, and the residues interactions between antigen and antibody binding site were shown in Fig. 1d. There were hydrogen bond, ion bond or hydrophobic interactions between DLL4 residues: K189, K190, H194, F195, H197, W212, Q218, Q219 and MMGZ01 residues: HCDR1-W33, HFR2-W47, HCDR2-D55, HCDR2-D57, HCDR3-N100, HCDR3-F101, LCDR1-S32, LCDR3-W92. The interactive MMGZ01 residues were mostly located in CDRs excepted HFR2-W47, which was recommended to be retained in humanization.

**Humanization of MMGZ01 Fv.** With the precise structure of MMGZ01 Fv, we further identified the canonical residues in FRs which were important for CDR conformation maintaining or binding affinity of antibody. These canonical residues in FRs were shown in Table 2 and identified as 3 types: 1. VH-VL interface core residues: the major Fv dimer contact residues which may affect the orientation of VH and VL domains and

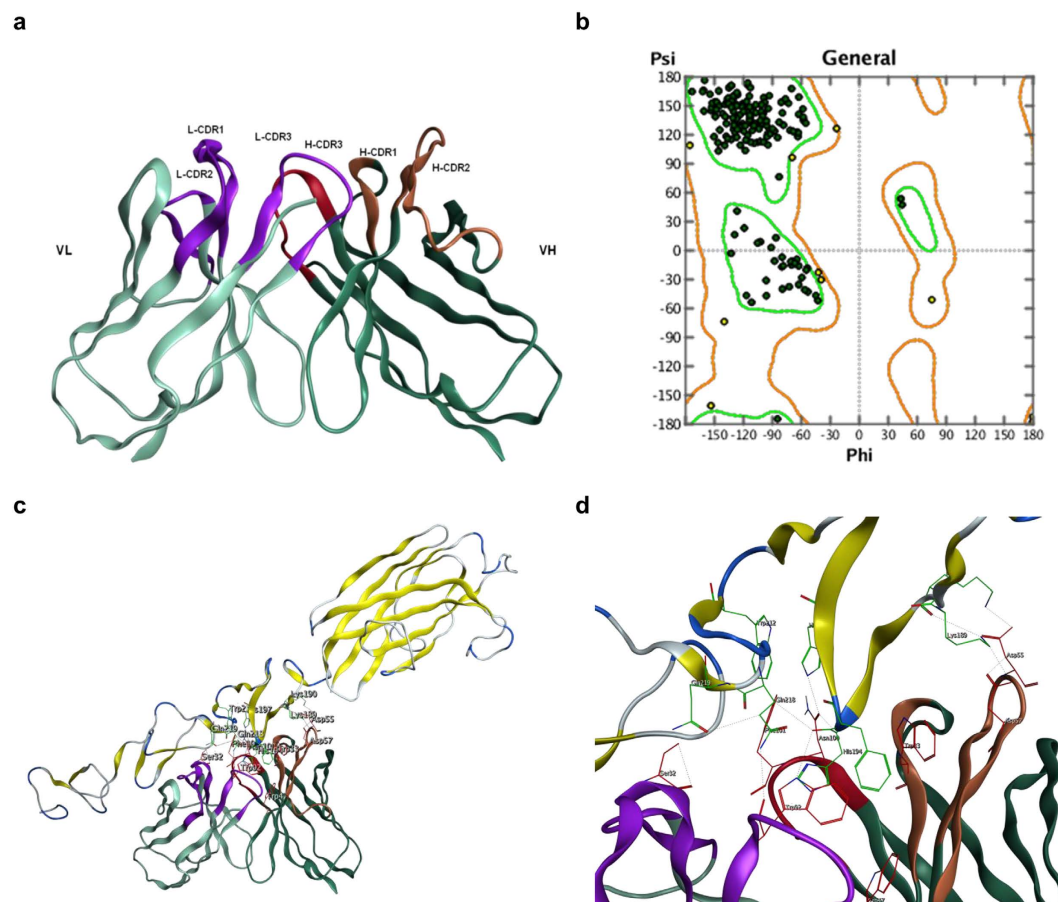


**Figure 1. Structure model of MMGZ01 Fv and complex structure with DLL4.** (a) 3D structure of the simulated MMGZ01 Fv. The structure was built in MOE with various antibody structures templates found in PDB database. (b) Structure evaluation with Ramachandran plot. Residues in the core regions are rendered green and residues in allowed regions are rendered yellow. (c) Complex structure of MMGZ01 Fv and DLL4 predicted by molecular docking. (d) Residues interaction in antibody-antigen binding site. Interactive residues located in antibody are rendered red and those located in DLL4 are rendered green. DLL4 **K189** had hydrogen bond with HCDR2-D57, ion bond with HCDR2-D55 and D57. DLL4 **K190** had ion bond with HCDR2-55D. DLL4 **H194** had hydrogen bond with LCDR3-W92 and HCDR3-N100. DLL4 **F195** had hydrophobic interaction with LCDR3-W92, HCDR1-W33 and HFR2-W47. DLL4 **H197** had hydrogen bond with HCDR3-N100. DLL4 **W212** had hydrophobic interaction with HCDR3-F101. DLL4 **K218** had hydrogen bond with LCDR3-W92. DLL4 **Q219** had hydrogen bond with LCDR1-S32.

Position	Residues	Interface core	Loop foundation	Loop interaction
LFR1	I4	0	1	1
LFR2	P47	1	1	0
LFR2	W48	0	1	0
LFR2	Y50	1	1	1
LFR3	Y72	0	1	1
HFR1	Y27	0	1	0
HFR2	I37	1	1	1
HFR2	K38	1	1	0
HFR2	I48	0	1	1
HFR3	A68	0	1	0
HFR3	L70	0	1	1
HFR3	G98	0	1	0

**Table 2. Canonical residues in FRs of VH & VL for back mutation.** 1 represents yes and 0 represents no, residues shown are original murine ones.





target affinity (Supplementary Fig. S3), emphasizing the importance of FR residues, in particular the 12 canonical residues in maintaining the binding affinity. Back mutations of these 12 canonical residues to the CDR grafting were essential in binding affinity recovery. Considering the principle of humanization - reducing immunogenicity, we expected to mutate less residues while retaining high affinity. Thus, the importance of each of these 12 canonical residues to the MMGZ01 Fv structure was further evaluated by site-directed mutagenesis and prediction of stability changes<sup>24,25</sup>. If the mutations altered the stability too much, they may cause the loss of the antibody's structure and function. In each mutation, the murine residue were mutate to the corresponding one in VH<sub>g</sub> or VL<sub>g</sub>, and change in stability from mutant antibody to the wild type was reported and expressed as dStability. When generating an ensemble, dStability is equal to the Boltzman average of the relative stabilities of the ensemble. As shown in Supplementary Table S1, a more positive dStability value indicated a more unstable mutation<sup>24,25</sup>, and these canonical residues were recommended to back mutate to the murine one after CDR grafting.

From the above, canonical residues belonged to all the 3 types and/or with dStability most positive were extremely important and back mutated to the corresponding murine one with priority, residues less important were gradually added and back mutated in the latter version (see Supplementary Fig. S2). Through transient transfection, the humanized antibodies were expressed in CHO-s cell, and the binding activity was analyzed and compared by ELISA assay. As shown in Supplementary Fig. S3, the humanized antibody (H<sub>3</sub>L<sub>2</sub>) which back mutated all the 12 residues possessed the most similar antigen binding activity with the chimeric antibody H<sub>C</sub>L<sub>C</sub>. The amino acid sequences of H<sub>3</sub>L<sub>2</sub> were shown in Fig. 2a,b.

**Structural comparison between MMGZ01 and H<sub>3</sub>L<sub>2</sub> Fv.** Superposition is a useful tool for comparing protein structures and the RMSD value reflects conformation difference<sup>26</sup>. The 3-D structure of H<sub>3</sub>L<sub>2</sub> Fv was modeled as described above, structure templates and sequence similarities were shown in Supplementary Table S2. Then the structure of H<sub>3</sub>L<sub>2</sub> Fv were superposed with the parent MMGZ01 Fv structure and structural Root Mean Square Deviation (RMSD) were calculated. The resulting superposition model was shown in Fig. 2c, and the RMSD value between the superposed Fv structures was 0.824 Å. The results indicates that H<sub>3</sub>L<sub>2</sub> Fv had a similar conformation with the parent MMGZ01 Fv.

**Stable expression and purification of H<sub>C</sub>L<sub>C</sub> and H<sub>3</sub>L<sub>2</sub>.** After 2-round screening of stable transfectants<sup>27</sup>, we finally got 4 clones with highest expression levels of H<sub>C</sub>L<sub>C</sub> or H<sub>3</sub>L<sub>2</sub>. Clones produced about 5 mg/L H<sub>C</sub>L<sub>C</sub> or 7 mg/L H<sub>3</sub>L<sub>2</sub> were cultured and supernatant was purified by Protein A affinity chromatography. The purified protein was analyzed by Western Blot and SDS-PAGE. As shown in Fig. 3a,b, H<sub>C</sub>L<sub>C</sub> and H<sub>3</sub>L<sub>2</sub> shared the expected molecular weight of 156 KDa in non-reduced condition and 52/26 KDa in reduced condition.

**Affinity of H<sub>3</sub>L<sub>2</sub> to rhDLL4.** To better evaluate the binding affinity and kinetics of H<sub>3</sub>L<sub>2</sub> to rhDLL4, an SPR-based assay was used. H<sub>C</sub>L<sub>C</sub> or H<sub>3</sub>L<sub>2</sub> was captured by a capture antibody immobilized onto the biosensor chip surface. Then gradient concentrations of rhDLL4 up to 100 nM were passed through the surface. The recorded sensorgrams were fitted with a 1:1 binding model (Fig. 3c,d), and the equilibrium constant  $K_D$  of H<sub>3</sub>L<sub>2</sub> calculated from ratio of  $k_d/k_a$  was  $2.26 \times 10^{-12}$  M, which is comparable to that of H<sub>C</sub>L<sub>C</sub> ( $1.41 \times 10^{-12}$  M). The humanized antibody H<sub>3</sub>L<sub>2</sub> exhibited high affinity and specificity to rhDLL4 which were similar to that of its parental antibody.

**Binding capacity to HUVEC cells.** HUVEC is an endothelial cell line shown to express DLL4 ligand<sup>28</sup>. To investigate if H<sub>3</sub>L<sub>2</sub> could bind to DLL4 ligand natively expressed on cells, we used Flow Cytometry to detect binding capacity of H<sub>3</sub>L<sub>2</sub> to HUVEC cells. As shown in Fig. 4a, binding rates of 10 µg/ml H<sub>3</sub>L<sub>2</sub> or H<sub>C</sub>L<sub>C</sub> with HUVEC cells were 36.9% and 38.1% respectively. Low binding of H<sub>3</sub>L<sub>2</sub> or H<sub>C</sub>L<sub>C</sub> to the DLL4 negative cell line HEK-293 was observed (1.72%, 0.46%). This results indicates that H<sub>3</sub>L<sub>2</sub> specifically bound to DLL4 expressed on HUVEC cells, and its binding capacity was comparable to that of H<sub>C</sub>L<sub>C</sub>.

**H<sub>3</sub>L<sub>2</sub> promotes HUVEC cells proliferation through inhibition of DLL4 directed Notch signaling.** Prior to HUVEC cells seeding, rhDLL4 was immobilized onto 96-well plates to simulate Notch receptor of adjacent cells<sup>29,30</sup>. rhDLL4 caused growth inhibition of HUVEC cells compared to plates without rhDLL4, and H<sub>3</sub>L<sub>2</sub> reversed this inhibition in a dose dependent manner (Fig. 4b). Notch intracellular domain (NICD) levels were analyzed as representative of Notch signaling activation<sup>4</sup>. In a Western Blot assay, H<sub>3</sub>L<sub>2</sub> led to significant NICD reduction in HUVEC cells in a dose dependent manner, and resulted in almost NICD elimination at concentration of 10 µg/ml ( $P = 0.000114$ ) (Fig. 4c,d). These results indicates that proliferation of HUVEC cells caused by H<sub>3</sub>L<sub>2</sub> was due to inhibition of DLL4 directed Notch signaling.

**H<sub>3</sub>L<sub>2</sub> modulates angiogenesis and inhibit tumor growth.** Studies show that DLL4 is selectively expressed by intratumoral endothelial cells in breast cancer but not in normal breast tissue<sup>31</sup>, and aberrant activation of Notch signaling is associated with breast carcinogenesis<sup>32,33</sup>. To evaluate the *in vivo* anti-tumor activity of H<sub>3</sub>L<sub>2</sub>, a MDA-MB-231 breast cancer xenograft model was used. After implantation, tumor cells were allowed to grow for about 10 days before the tumor volume reached 100 mm<sup>3</sup>. Treatment of H<sub>3</sub>L<sub>2</sub> on these tumor-bearing mice obtained maximal tumor inhibition rates of 35% and 59% at dose of 2.5 mg/kg and 5 mg/kg respectively. As a reference for humanized antibody, 5 mg/kg chimeric antibody H<sub>C</sub>L<sub>C</sub> was shown to achieve the similar tumor inhibition rate (56%) with the same dose of H<sub>3</sub>L<sub>2</sub> ( $P = 0.406$ ) (Fig. 5a,b).

The effect of H<sub>3</sub>L<sub>2</sub> on mitotic index (Ki67) and apoptosis (cleaved caspase-3) in the tumor was detected by immunohistochemical staining. A distinct increase in cleaved caspase-3 and a reduction of Ki67 level were observed with treatment of H<sub>3</sub>L<sub>2</sub>, which indicates that H<sub>3</sub>L<sub>2</sub> inhibited tumor cells proliferation and induced apoptosis of tumor cells (Fig. 5e,g). Angiogenesis in the tumor was further analyzed by immunofluorescence, where treatment of H<sub>3</sub>L<sub>2</sub> result in increase in vessel number, along with a reduction in percentage of α-SMA-positive (α-SMA+) mural cells (Fig. 5f,h). This result was consistent with H<sub>3</sub>L<sub>2</sub> caused endothelium cell proliferation,

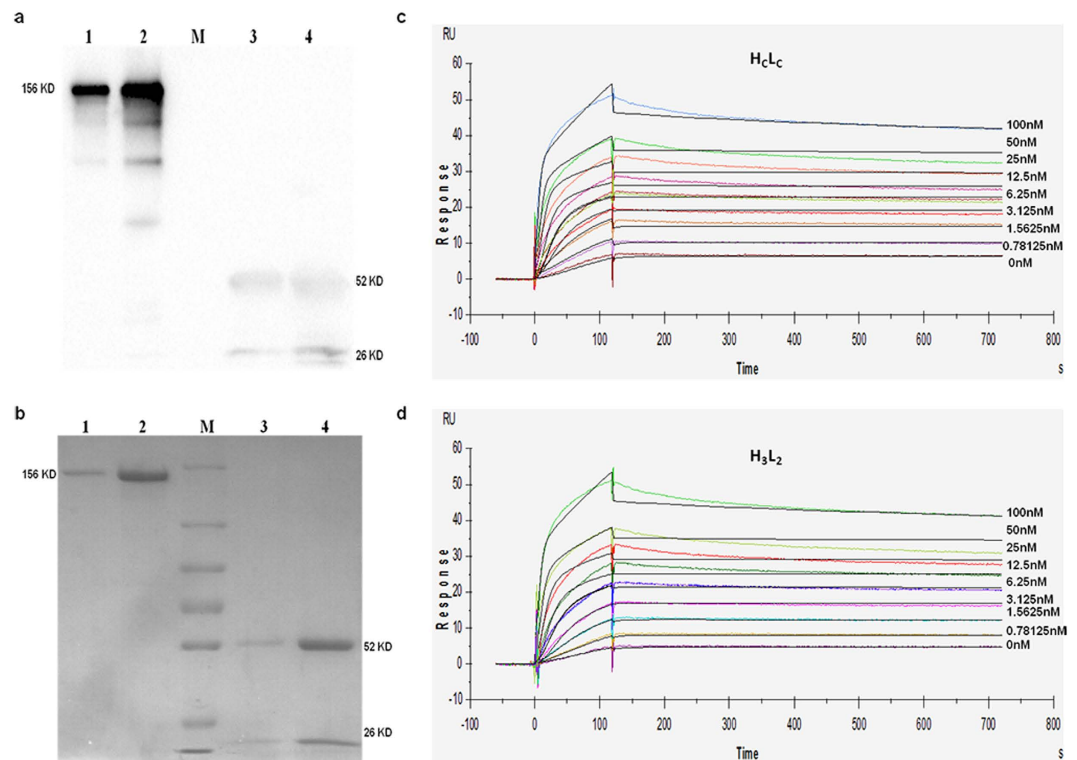


**Figure 3. Expression, purification and antigen binding kinetics of chimeric or humanized antibody.**

(a) SDS-PAGE and (b) Western Blot assay of stable expressed and purified H<sub>c</sub>L<sub>c</sub>/H<sub>3</sub>L<sub>2</sub>. Lane 1 and 3 were non-reduced and reduced H<sub>c</sub>L<sub>c</sub>, lane 2 and 4 were non-reduced and reduced H<sub>3</sub>L<sub>2</sub> respectively. Lane M were marker with molecular weight of 250, 130, 100, 70, 55, 35, 25 KDa. (c,d) Antigen binding kinetics analyzed by SPR. Sensorgrams of series concentrations of rhDLL4 binding to (c) H<sub>c</sub>L<sub>c</sub> or (d) H<sub>3</sub>L<sub>2</sub> were recorded and fitted with a 1:1 binding model.  $k_d$  and  $k_a$  of H<sub>c</sub>L<sub>c</sub> were  $2.42 \times 10^{-5}$  1/s and  $1.72 \times 10^7$  1/Ms, and  $K_D$  calculated from  $kd/ka$  was  $1.14 \times 10^{-12}$  M.  $R^2$  value of H<sub>c</sub>L<sub>c</sub> was 1.44 and  $R_{max}$  was 50.77 RU.  $k_d$  and  $k_a$  of H<sub>3</sub>L<sub>2</sub> were  $2.59 \times 10^{-5}$  1/s and  $1.15 \times 10^7$  1/Ms, and  $K_D$  was  $2.26 \times 10^{-12}$  M.  $R^2$  value of H<sub>3</sub>L<sub>2</sub> was 1.68 and  $R_{max}$  was 50.9.

while lack of mural cells led to immature vessels<sup>34,35</sup> (CD31+/α-SMA-). Different from H<sub>3</sub>L<sub>2</sub> induced increment of neoangiogenic vessels, tumors treated with vehicle control showed less vessels but all coated with mural cells (CD31+/α-SMA+). Reduction of NICD levels in the same tumor samples were observed in Western Blot assay (Fig. 5c,d). In conclusion, H<sub>3</sub>L<sub>2</sub> demonstrated an anti-tumor effect *in vivo* through promotion of dysfunctional angiogenesis and cell apoptosis in tumor.

## Discussion

The aim of this study is to humanize a murine antibody MMGZ01 targeting DLL4 and evaluate its anti-tumor activity. The ultimate purpose of humanization is to substitute murine residues with human residues to reduce immunogenicity while retaining the original binding affinity to the maximum. The antigen binding affinity mainly depends on six CDRs which are shaped and supported by the relatively conserved FRs in the variable regions. CDR grafting from murine to human FR templates with highest similarity is a widely used method for humanization. In this study, the optimal human FR templates were screened by structure-based computational method. Studies show that chimeric antibody usually shares the similar binding affinity with the original murine antibody<sup>16,36</sup>. Meanwhile, the human constant regions of chimeric antibody make it more convenient for detection in parallel experiments, so we designed and generated a chimeric antibody (H<sub>c</sub>L<sub>c</sub>) as positive reference for humanized antibodies.

Firstly, a precise MMGZ01 Fv structure was obtained based on antibody structure templates for all subdomains (CDR1-3 and FR1-4). The sequence similarities and structure fitness of templates were comprehensively scored by MOE (Fig. 1a, Table 1). According to the Fv structure, canonical residues were identified and categorized into 3 types: VH-VL interface core residues which were important for dimer packing; CDR loop foundation residues buried directly underneath the CDRs<sup>23</sup> and CDR loop interaction residues directly contacted with the CDR residues (hydrogen, hydrophobic or ion bond) (Table 2). These crucial residues were considered to be retained from the murine antibody in CDR grafting. The antigen epitope recognized by MMGZ01 was screened from a dodecapeptide phage display library, and selected in DLL4 before docking with MMGZ01 Fv. The complex structure predicted through docking approach provided important residues interactions in the antibody-antigen binding site. Further the interactive residues in MMGZ01 Fv were also recommended to be retained in humanization. Moreover, the interactive residues in CDRs may be designated as specificity-determining residues (SDRs),

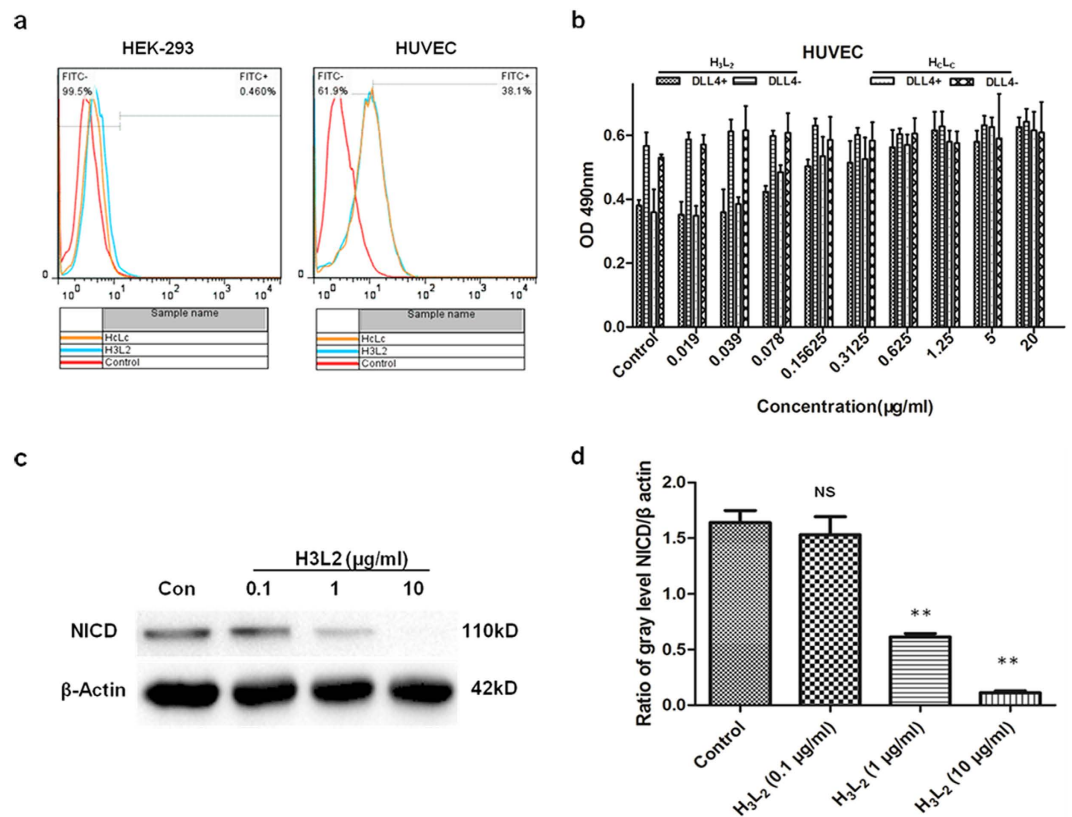


**Figure 4. Effects of H<sub>3</sub>L<sub>2</sub> on HUVEC cells.** (a) Binding capacity to HUVEC cells analyzed by Flow Cytometry. H<sub>3</sub>L<sub>2</sub> and H<sub>C</sub>L<sub>C</sub> exhibited similar binding rates to HUVEC cells (36.9% and 38.1% respectively), and low binding to HEK-293 was observed (1.72% and 0.46% respectively). (b) H<sub>3</sub>L<sub>2</sub> promoted HUVEC cells proliferation in a dose dependent manner. Cell proliferation were measured by MTT method and shown as absorbance units (mean ± SD, n = 3). (c,d) NICD levels in HUVEC cells detected by Western Blot. H<sub>3</sub>L<sub>2</sub> inhibited Notch1 activation in a dose gray dependent manner. (d) Ratio of NICD and β actin gray levels. Gray levels were analyzed by Alpha Ease FC™ software, version 3.1.2. Data are given as the mean ± SD (n = 3). NS: no significance, \*\**p* ≤ 0.01 versus Control.

and used for SDRs grafting. This new approach of antibody humanization may further reduce the anti-variable region or anti-idiotypic responses caused by xenogeneic CDR<sup>37</sup>, and is our plan for future work.

The humanization of MMGZ01 was started with CDR grafting. Human V or J genes with highest sequence similarity and most canonical residues conserved were chosen for CDR grafting. Although most canonical residues were conserved, there were still some differed (Fig. 2, Table 2), and evidence showed that the CDR grafting antibody was not able to retain the antigen binding activity (Supplementary Fig. S3). To evaluate the contribution of these differed canonical residues to antigen binding, we introduced a number of back mutations to the CDR grafting antibody (see Supplementary Material). The humanized antibody (H<sub>3</sub>L<sub>2</sub>) which back mutated all the 12 residues showed similar antigen binding capacities with the chimeric antibody H<sub>C</sub>L<sub>C</sub> (Supplementary Fig. S3). Meanwhile, 3D structure of H<sub>3</sub>L<sub>2</sub> was also built and superposed with the MMGZ01 Fv structure. The calculated structural RMSD (0.824 Å) indicated a similar conformation between the two antibodies. Experimental results were consistent with the computational predictions, thus we confirmed the importance of FRs canonical residues identified here. In addition, the efficient and reliable approach for humanization proposed in this study, which combined computational modeling with experiments, could be applied to the humanization of other antibodies.

Stable transfectants expressing H<sub>3</sub>L<sub>2</sub> were introduced by electroporation and screened by G418. The purified H<sub>3</sub>L<sub>2</sub> showed expected molecular weight in reduced and non-reduced condition, indicating an integrated assembly of the antibody (Fig. 3a,b). To investigate the binding specificity and affinity of H<sub>3</sub>L<sub>2</sub> to DLL4, we used the SPR-based method which provide sensorgrams visualizing all the data from an interaction in real time. Our results indicates that H<sub>3</sub>L<sub>2</sub> retained the high specificity and affinity from its parental antibody (Fig. 3c,d).

Moreover, the effects of H<sub>3</sub>L<sub>2</sub> on DLL4 positive cells were investigated with HUVEC cells. As a normal endothelium cell line, HUVEC expresses relatively lower level of DLL4 compared to tumor vessels<sup>28</sup>. We found that addition of rhDLL4 inhibited proliferation of HUVEC cells, while H<sub>3</sub>L<sub>2</sub> effectively reversed this inhibition (Fig. 4b). Furthermore, NICD, as the activated form of Notch receptor, was significantly decreased in the treatment of H<sub>3</sub>L<sub>2</sub> (Fig. 4c,d). In conclusion, the humanized antibody H<sub>3</sub>L<sub>2</sub> effectively blocked the DLL4-Notch signaling pathway and further promoted the proliferation of HUVEC cells *in vitro*.



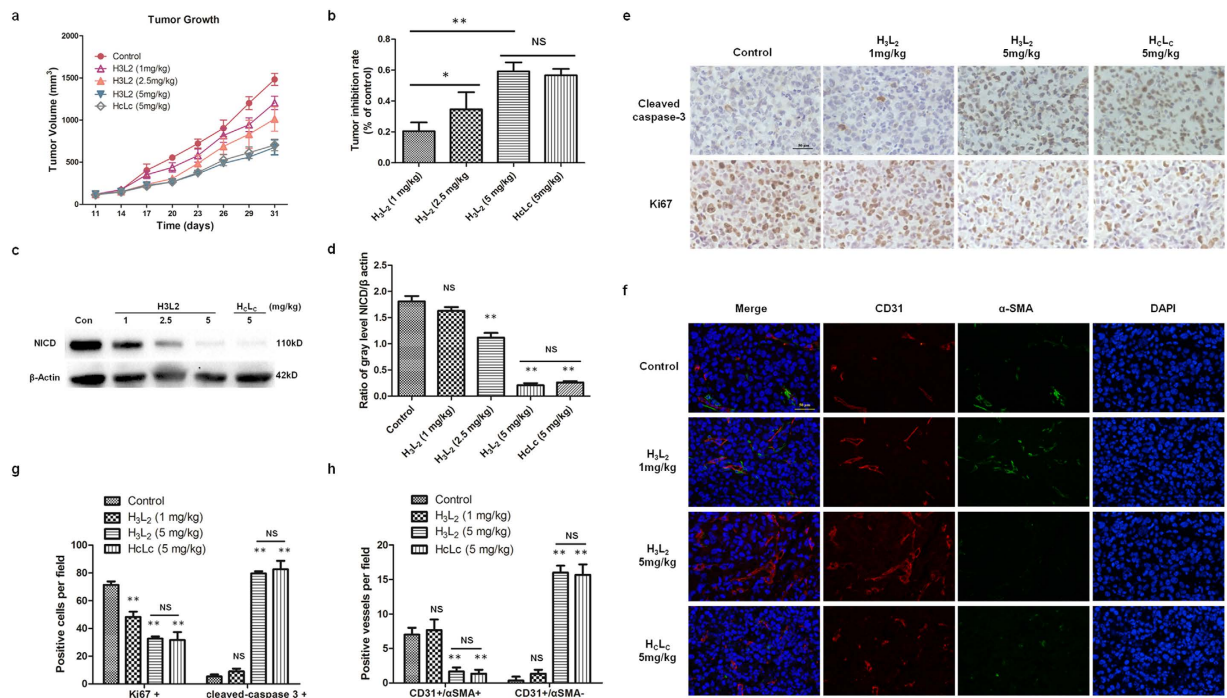


**Figure 5.** The *in vivo* anti-tumor activity of H<sub>3</sub>L<sub>2</sub> in the MDA-MB-231 xenograft model. (a) Tumor growth curves of nude mice in different groups. 30 nude mice were randomly divided into 5 groups for drug administration on the 11th day post tumor cell inoculation, tumor volumes of mice were measured with the mean  $\pm$  SD,  $n = 6$ . (b) Tumor inhibition rates of different groups. Average tumor inhibition rates of each group were 19% (H<sub>3</sub>L<sub>2</sub> 1 mg/kg), 34% (H<sub>3</sub>L<sub>2</sub> 2.5 mg/kg), 59% (H<sub>3</sub>L<sub>2</sub> 5 mg/kg) and 56% (H<sub>c</sub>L<sub>c</sub> 5 mg/kg). Data are given as the mean  $\pm$  SD ( $n = 6$ ). (c) NICD levels in tumor cells analyzed by Western Blot. (d) Ratio of NICD and  $\beta$  actin gray levels. Gray levels were analyzed by Alpha Ease FC<sup>TM</sup> software, version 3.1.2. Data are given as the mean  $\pm$  SD ( $n = 3$ ). (e) Expression levels of Ki67, cleaved caspase-3 (brown staining) in tumors analyzed by IHC. Photomicrographs were taken at 400x magnifications. Scale bar = 50  $\mu$ m. (g) Quantifications of Ki67 or cleaved caspase-3 positive cells per field. Data are given as the mean  $\pm$  SD ( $n = 3$ ). (f) Immunofluorescence double staining of CD31-positive (red fluorescence) and  $\alpha$ -SMA-positive (green fluorescence) cells in tumors. Scale bar = 50  $\mu$ m. (h) Quantifications of mature (CD31+/ $\alpha$  SMA+) or immature (CD31+/ $\alpha$  SMA-) vessels per field. Data are given as the mean  $\pm$  SD ( $n = 3$ ). \* $p \leq 0.05$ , \*\* $p \leq 0.01$ , NS: no significance.

DLL4 is unregulated by intratumoral endothelial cells in most breast cancer<sup>31</sup>, and aberrant activation of Notch signaling is associated with breast carcinogenesis<sup>32,33</sup>. When endothelial cells form the inner vessel wall, mural cells associate with and coat the endothelial cell tube to make mature and functional vessels<sup>34,35</sup>. In this study, a MDA-MB-231 xenograft model was established to evaluate the *in vivo* anti-tumor activity of H<sub>3</sub>L<sub>2</sub>. The results indicate that H<sub>3</sub>L<sub>2</sub> inhibited tumor growth through blockage of DLL4-Notch signaling pathway (Fig. 5a–d). In the presence of H<sub>3</sub>L<sub>2</sub>, increase in vessel number along with a reduction in percentage of mural cells was observed (Fig. 5f,h). Thus, the vessels induced by H<sub>3</sub>L<sub>2</sub> were immature and dysfunctional, which contributed to the inhibition of tumor growth. In addition, the observed increase in expression of cleaved caspase-3 along with decrease in Ki67 (Fig. 5e,g) indicates that H<sub>3</sub>L<sub>2</sub> mediated tumor inhibition was associated with induction of tumor cell apoptosis and inhibition of tumor cell proliferation.

In summary, H<sub>3</sub>L<sub>2</sub> is an ideal humanized antibody that blocks DLL4/Notch pathway against breast carcinoma *in vivo* and it is a promising anti-tumor drug candidate for clinical studies.

## Methods

**Materials.** Restriction enzymes were purchased from NEB (New England Biolabs, Ipswich, MA, USA). T4 DNA Ligase was purchased from Thermo Scientific (Shanghai, China). Eukaryotic expression vectors pMH3-H, pCApuro-H, pMH3-L, pCApuro-L contained full-length IgG1 H & L chain were preserved in our lab<sup>27</sup>. Chinese hamster ovary (CHO-s) cell line was purchased from AmProtein (Hangzhou, Zhejiang, China) and cultured in DMEM/F12 medium with 10% (v/v) fetal bovine serum (FBS). HUVEC cells purchased from ScienCell research laboratories (Carlsbad, CA, USA) were cultured in ECM medium supplement with 5% (v/v) FBS and 1% (v/v) ECGS (ScienCell, San Diego, CA, USA). Cell culture media and trypsin powder were purchased from Life Technologies (Basel, Switzerland).

**Cloning of VH and VL genes of MMGZ01.** The total RNA of MMGZ01 hybridoma cell line was isolated using a Trizol reagent (Invitrogen, Burlington, ON, Canada), and reverse-transcribed to cDNA with a M-MuLV RT-PCR kit (Sangon Biotech, Shanghai, China). In the Polymerase Chain Reaction (PCR), PrimeSTAR HS DNA



polymerase was used to amplify the VH and VL genes with designed degenerate primers specific for murine antibodies (Takara Bio, Dalian, Liaoning, China). Chains of VH and VL were detected in a 1% agarose gel and corresponding bands were purified using an Agarose Gel Extraction Kit (Takara Bio, Dalian, Liaoning, China). The purified chains were then cloned to pMD18T vector for sequencing (Genscript Corporation, Nanjing, Jiangsu, China).

**Antibody modeling and evaluation.** The 3D structure model of MMGZ01 Fv was built by antibody homology modeling method<sup>38</sup> using chemical computing and molecular modeling software, Molecular Operating Environment (MOE), version 2013.08, where we searched antibody structure templates in PDB database for each subdomains. Templates for FRs in VH & VL or the VH-VL dimer were searched by sequence identity, and the CDR regions by sequence similarity.

The Fv model of MMGZ01 was built with the Antibody Builder according to the templates found, then refined to relieve strained geometry and further applied energy minimization scheme in Amber 10:EHT force field and achieved a final structure model<sup>39</sup>. This resulting Fv structure was tested on stereo-chemical quality with Protein Geometry in MOE. Backbone Bond lengths, angles and dihedrals were compared to averages and standard deviations of a reference database of high resolution structures from the PDB<sup>18</sup>.

As the precise structure of Fv was established, we further identified the canonical residues in FRs which were important for CDR conformation maintaining or the binding affinity of antibody. These canonical residues could be classified into 3 types: the VH-VL interface core residues<sup>23</sup> (distance = 5.00 Å, buried percentage >85%), the CDR loop foundation residues (radius = 5.00 Å, buried percentage >85%) and the CDR loop interaction residues (cutoffs = 5.00 Å).

**Epitope mapping by randomized dodecapeptide phage display library.** Epitope mapping of MMGZ01 antibody was directed with the Ph.D.<sup>TM</sup>-12 Phage Display Peptide Library Kit (New England Biolabs, Ipswich, MA, USA). In the panning,  $1.5 \times 10^{10}$  phages were incubated with a plate coated with MMGZ01 for 2 h at 37°C, after washing away the unbound phages, the specifically bound phages were eluted with Glycine - HCl (pH 2.2) and amplified in *E. coli* ER2738 in the logarithmic phase for another binding - amplification cycle. After 4 cycles, individual clones were amplified and characterized by ELISA. Detected with HRP-conjugated anti-M13 monoclonal antibody (Sino Biological Inc. Beijing, China), the DNA of positive clones was isolated and sequenced by Genscript Corporation (Nanjing, Jiangsu, China).

**Molecular docking.** The structure of DLL4 were downloaded from SWISSMODEL. Epitope recognized by MMGZ01 were selected as contact residues in DLL4 before docking. A rigid protein docking program ZDOCK<sup>21,22</sup> sever (version ZD3.0.2) was used, and MMGZ01 Fv was set as receptor structure, DLL4 was set as ligand structure. The top modeled complex structure was analyzed by MOE.

**Humanization of MMGZ01 Fv.** The humanization of MMGZ01 Fv contained two steps of design: First, grafted the CDR regions onto the FR regions of human immunoglobulin germline V and J gene to get a CDR grafted Fv; Second, chose the changed canonical residues in FR regions to back mutate to the original murine ones. We searched the human immunoglobulin germline V genes for templates of FR1-3. The human donor V genes with highest FR sequence similarity and most canonical residues conserved were selected. Human donor J genes provided for templates of FR 4 were selected based on their highest VH & VL CDR3 similarity and canonical residues in FR4. Then, a CDR grafted Fv (VH<sub>g</sub>, VL<sub>g</sub>) was archived by grafting MMGZ 01 VH & VL CDRs onto FRs of human donors V and J genes.

Although the most canonical residues conserved templates were selected, there were some canonical residues changed, which were candidates for back mutation. The humanized Fv based on CDR grafting and back mutation with all the candidates was named as H<sub>3</sub>L<sub>2</sub> Fv (VH<sub>3</sub>, VL<sub>2</sub>).

**Construction and transient expression of chimeric or humanized antibodies.** The VH & VL of MMGZ01 or humanized antibodies were added Kozak sequence, signal peptide and restriction enzyme cutting sites, then optimized to CHO-preferred codons, synthesized and cloned to pUC57-simple vectors by Genscript Corporation (Nanjing, Jiangsu, China) respectively. Restriction enzyme cutting site in VH were *EcoRI* & *NheI*, and in VL were *EcoRI* and *SalI*. Expression vectors (pMH3-H, pCApuro-H, pMH3-L, pCApuro-L) with the corresponding cutting site between VH and CH or between VL and CL<sup>27</sup> were used. After double digestion and ligation of these vectors, VH & VL of MMGZ01 or humanized antibodies were cloned to pMH3 and pCA-puro replacing VH & VL of IgG1 to join full-length chimeric (H<sub>C</sub>L<sub>C</sub>) or humanized antibodies. Nucleotide sequences of recombinant H-chain and L-chain vectors were confirmed with sequencing by Genscript Corporation (Nanjing, Jiangsu, China).

The recombinant expression vectors of H<sub>C</sub>L<sub>C</sub> or humanized antibodies were then transient transfected into CHO-s cells using SuperFectin II Transfection Reagent (Pufei Biotech Co., Ltd, Shanghai, China). After 72 h incubation, the supernatant was collected and analyzed by ELISA (see Supplementary Material).

**Structure superposition and RMSD calculation.** The 3-D structure model of H<sub>3</sub>L<sub>2</sub> Fv was built and superposed with the structure model of MMGZ01 Fv. Structure RMSD between corresponding protein alpha carbons (C $\alpha$ ) were calculated in MOE, where a weighted non-linear optimization was used to determine the solid-body transformations required to maximize the superposition of the protein atomic coordinates<sup>26</sup>.

**Stable expression and purification of H<sub>C</sub>L<sub>C</sub> or H<sub>3</sub>L<sub>2</sub>.** Expression vectors of H<sub>C</sub>L<sub>C</sub> or H<sub>3</sub>L<sub>2</sub> were transfected to CHO-s cells by electroporation and stable transfectants were screened using the method previously

described<sup>27</sup>. Clones producing highest amount of antibodies were grown in medium with 5% FBS and purified by Protein A affinity chromatography (GE Healthcare, Buckinghamshire, UK).

**Affinity analysis.** The binding kinetics of H<sub>C</sub>L<sub>C</sub> or H<sub>3</sub>L<sub>2</sub> to rhDLL4 were analyzed using an Surface Plasmon Resonance (SPR)-based assay on Biacore X100 system (GE Healthcare, Buckinghamshire, UK). An anti-human IgG Fc antibody (GE Healthcare, Buckinghamshire, UK) was firstly immobilized onto a CM5 biosensor chip. Then, appropriate concentration of H<sub>C</sub>L<sub>C</sub> or H<sub>3</sub>L<sub>2</sub> was captured to the surface with an increase of Resonance Unit (RU) up to 2,000. Finally, various concentrations of rhDLL4 were passed through the chip. After each reaction, the captured H<sub>C</sub>L<sub>C</sub> or H<sub>3</sub>L<sub>2</sub> antibody and analyte were removed by Regeneration (3 M magnesium chloride). The whole reaction was conducted at 25 °C and flow rate of 30 μl/min. Sensorgrams of each concentration were obtained and analyzed by Biacore evaluation software (GE Healthcare, Buckinghamshire, UK). The equilibrium constant  $K_D$  was calculated from ratio of dissociation rate constant  $k_d$  to association rate constant  $k_a$  ( $k_d/k_a$ ).

**Flow cytometry.**  $4 \times 10^5$  HUVEC cells cultured in ECM were digested by trypsin and resuspended in PBS containing 2% FBS. Then the cells were washed and incubated with 10 μg/ml H<sub>C</sub>L<sub>C</sub> or H<sub>3</sub>L<sub>2</sub> at 4 °C for 1 h, followed by FITC conjugated donkey-anti-human IgG H+L (Sangon Biotech, Shanghai, China). Cells incubated with secondary antibody were used as background fluorescence control.  $1 \times 10^4$  cells were analyzed in all individual detections. The binding assay was performed on a BD FACS flow cytometry and the obtained data was processed using FlowJo 7.6 software.

**Cell proliferation assay.** 96-well plates immobilized with 1 μg/ml rhDLL4 or PBS were seeded with  $4 \times 10^3$  HUVEC cells, meanwhile, series concentrations of H<sub>C</sub>L<sub>C</sub> or H<sub>3</sub>L<sub>2</sub> were added into the plates, each concentration has three repeats. Same volume PBS was added as control. After incubation for 72 h, cell viability was determined by MTT assay.

**Notch signaling blockage analyzed by Western Blot.** 6-well plate immobilized with 1 μg/ml rhDLL4 was seeded with  $5 \times 10^5$  HUVEC cells, meanwhile, H<sub>C</sub>L<sub>C</sub> or H<sub>3</sub>L<sub>2</sub> were added to final concentrations of 0.1, 1, 10 μg/ml. After incubation for 24 h, the cells were lysed and extracts were harvested by RAPI buffer (Beyotime, Shanghai, China). About 20 μg of extracts were resolved by electrophoresis and then transferred onto PVDF membranes. The membranes were then blocked and incubated with cleaved Notch1 (Val1744) antibody (Cell Signaling Technology, Boston, MA, USA) or anti-β-actin (Anbo Manufacturing, Colville, WA, USA), followed by incubation of HRP conjugated goat-anti-rabbit antibody (Signalway Antibody LLC, College Park, MD, USA). Finally, after reacting with ECL substrates, the membrane was analyzed by Bio-Rad GelDoc™ XR+ system.

**Human tumor xenograft model and drug administration.** The human breast cancer cell line MDA-MB-231 was obtained from ATCC and the cells were cultured in DMEM medium supplement with 10% FBS.  $1 \times 10^7$  MDA-MB-231 cells suspended in 100 μl PBS were subcutaneously injected into the left flank of 8-week old male nude mice. When the tumor volume reached about 100 mm<sup>3</sup>, the tumor-bearing mice were randomized and divided into groups for control (PBS) and different doses of H<sub>3</sub>L<sub>2</sub> (low dose: 1 mg/kg, middle dose: 2.5 mg/kg and high dose: 5 mg/kg), each group contained 6 mice. 5.0 mg/kg chimeric antibody was used as comparison for H<sub>3</sub>L<sub>2</sub> and antibodies were intravenously administrated every other day. Meanwhile, tumor volumes were measured every third day using a vernier caliper applying the formula  $V = LW^2/2$  (L is the long axis and W is the short axis of the tumor).

On the final day of study, percent (%) inhibition rates (IR) were calculated as  $IR\% = 100 \times (1 - V_t/V_c)$ , where  $V_t$  is average elevated volume of drug-treated group, and  $V_c$  is average elevated volume of control group. After 3 weeks' treatment, the mice were sacrificed and the tumors were prepared for analysis. All experiments were approved by the Animal Ethics Committee and were performed in accordance with the animal experiment center guidelines of Comparative Medicine Center of Yangzhou University.

**Immunohistochemical staining and immunofluorescence.** 4% paraformaldehyde fixed, paraffin embedded tumor tissues were cut to 5 μm thick sections for immunohistochemical (IHC) staining or immunofluorescence (IF). After rehydration, antigen retrieval and endogenous peroxidases quenching, the sections were blocked and further incubated with primary antibodies followed by corresponding secondary antibodies conjugated with HRP (for IHC) according to the instruction of Vectastain ABC Kit (Dako, Copenhagen, Denmark). The primary antibodies used were anti-Ki67, anti-cleaved caspase-3, anti-CD31 and anti-α-SMA (Cell Signaling Technology, Boston, MA, USA). For IF, cell chromosome was stained with 4',6'-diamidino-2-phenylindole (DAPI) and shown as blue. In addition, CD31-positive cells were shown as red, and α-SMA-positive were shown as green. Tumor sections were viewed and photographed using the Zeiss Axio Vert A1 microscope (Carl Zeiss, Thornwood, NY, USA).

**Statistical analysis.** Statistical analysis and variable slopes were performed with GraphPad prism software (GraphPad software Inc., La Jolla, CA, USA). Significance levels were estimated using the two-tailed student's t test and *P* values of 0.05 or less were considered statistically significant.

## References

- Nickoloff, B. J., Osborne, B. L. & Miele, L. Notch signaling as a therapeutic target in cancer: a new approach to the development of cell fate modifying agents. *Oncogene*. **22**, 6598–6608 (2003).
- Espinoza, I. & Miele, L. Notch inhibitors for cancer treatment. *Pharmacol Ther*. **139**, 95–110 (2013).
- Mailhos, C. *et al.* Delta4, an endothelial specific Notch ligand expressed at sites of physiological and tumor angiogenesis. *Differentiation*. **69**, 135–144 (2001).

4. Kuhnert, F., Kirshner, J. R. & Thurston, G. Dll4-Notch signaling as a therapeutic target in tumor angiogenesis. *Vascular Cell*. **3**, 20 (2011).
5. Mats, H. *et al.* Dll4 signalling through Notch1 regulates formation of tip cells during angiogenesis. *Nature*. **445**, 776–780 (2007).
6. Gavin, T., Irene, N. T. & Yancopoulos, G. D. The Delta paradox: DLL4 blockade leads to more tumour vessels but less tumor growth. *Nat Rev Cancer*. **7**, 327–331 (2007).
7. Scehnet, J. S. *et al.* Inhibition of Dll4-mediated signaling induces proliferation of immature vessels and results in poor tissue perfusion. *Blood*. **109**, 4753–4760 (2007).
8. Takebe, N., Nguyen, D. & Yang, S. X. Targeting Notch signaling pathway in cancer: Clinical development advances and challenges. *Pharmacol Ther*. **141**, 140–149 (2014).
9. Chiorean, E. G. *et al.* A Phase I First-in-Human Study of Enoticumab (REGN421), a Fully Human Delta-like Ligand 4 (Dll4) Monoclonal Antibody in Patients with Advanced Solid Tumors. *Clin Cancer Res*. **21**, 2695–2703 (2015).
10. Xu, Z. *et al.* MMGZ01, an anti-DLL4 monoclonal antibody, promotes nonfunctional vessels and inhibits breast tumor growth. *Cancer Lett*. **371**, 118–127 (2016).
11. Dhingra, K. *et al.* Phase I clinical and pharmacological study of suppression of human antimouse antibody response to monoclonal antibody L6 by deoxyspergualin. *Cancer Res*. **55**, 3060–3067 (1995).
12. Horneff, G., Winkler, T., Kalden, J. R., Emmrich, F. & Burmester, G. R. Human anti-mouse antibody response induced by anti-CD4 monoclonal antibody therapy in patients with rheumatoid arthritis. *Clin Immunol & Immunopathol*. **59**, 89–103 (1991).
13. Neuberger, M. S. *et al.* A hapten-specific chimaeric IgE antibody with human physiological effector function. *Nature*. **314**, 268–270 (1985).
14. Brüggemann, M., Winter, G., Waldmann, H. & Neuberger, M. S. The immunogenicity of chimeric antibodies. *J Exp Med*. **170**, 2153–2157 (1989).
15. Jones, P. T., Dear, P. H., Foote, J., Neuberger, M. S. & Winter, G. Replacing the complementarity-determining regions in a human antibody with those from a mouse. *Nature*. **321**, 522–525 (1986).
16. Presta, L. G. *et al.* Humanization of an anti-vascular endothelial growth factor monoclonal antibody for the therapy of solid tumors and other disorders. *Cancer Res*. **57**, 4593–4599 (1997).
17. Wu, T. T. & Kabat, E. A. An analysis of the sequences of the variable regions of Bence Jones proteins and myeloma light chains and their implications for antibody complementarity. *J Exp Med*. **132**, 211–250 (1970).
18. Dunbrack, R. L. Jr. & Cohen, F. E. Bayesian Statistical Analysis of Protein Sidechain Rotamer Preferences. *Protein Sci*. **6**, 1661–1681 (1997).
19. Lovell, S. C. *et al.* Structure Validation by C $\alpha$  Geometry:  $\phi$ ,  $\psi$  and C $\beta$  Deviation. *Proteins*. **50**, 437–450 (2003).
20. Stephen, C. W. & Lane, D. P. Mutant conformation of p53. Precise epitope mapping using a filamentous phage epitope library. *J Mol Biol*. **225**, 577–583 (1992).
21. Pierce, B. G. *et al.* ZDOCK server: interactive docking prediction of protein-protein complexes and symmetric multimers. *Bioinformatics*. **30**, 1771–1773 (2014).
22. Chen, R., Li, L. & Weng, Z. ZDOCK: An initial-stage protein-docking algorithm. *Proteins*. **52**, 80–87 (2003).
23. Ewert, S., Honegger, A. & Plückthun, A. Stability improvement of antibodies for extracellular and intracellular applications: CDR grafting to stable frameworks and structure-based framework engineering. *Methods*. **34**, 184–199 (2004).
24. Dehouck, Y. *et al.* Fast and accurate predictions of protein stability changes upon mutations using statistical potentials and neural networks: popmusic-2.0. *Bioinformatics*. **25**, 2537–2543 (2009).
25. Guerois, R., Nielsen, J. E. & Serrano, L. Predicting changes in the stability of proteins and protein complexes: a study of more than 1000 mutations. *J Mol Biol*. **320**, 369–387 (2002).
26. Shapiro, A., Botha, J. D., Pastore, A. & Lesk, A. M. A method for multiple superposition of structures. *Acta Crystallogr A*. **48**, 11–14 (1992).
27. Xie, W. *et al.* Generation and characterization of a novel human IgG1 antibody against vascular endothelial growth factor receptor 2. *Cancer Immunol Immunother*. **63**, 877–888 (2014).
28. Patel, N. S. *et al.* Up-regulation of delta-like 4 ligand in human tumor vasculature and the role of basal expression in endothelial cell function. *Cancer Res*. **65**, 8690–8697 (2005).
29. Wang, M. M. Notch signaling and Notch signaling modifiers. *Int J Biochem Cell B*. **43**, 1550–62 (2011).
30. Jenkins, D. W. *et al.* Med10639: a novel therapeutic antibody targeting DLL4 modulates endothelial cell function and angiogenesis *in vivo*. *Mol Cancer Ther*. **11**, 1650–1660 (2012).
31. Jubb, A. M. *et al.* Expression of vascular notch ligand delta-like 4 and inflammatory markers in breast cancer. *Am J Pathol*. **176**, 2019–2028 (2010).
32. Pece, S. *et al.* Loss of negative regulation by Numb over Notch is relevant to human breast carcinogenesis. *J Cell Biol*. **167**, 215–221 (2004).
33. Stylianou, S., Clarke, R. B. & Brennan, K. Aberrant activation of Notch signalling in human breast cancer. *Cancer Res*. **66**, 1517–1525 (2006).
34. Hirschi, K. K., Rohovsky, S. A., Beck, L. H., Smith, S. R. & D'Amore, P. A. Endothelial cells modulate the proliferation of mural cell precursors via platelet-derived growth factor-BB and heterotypic cell contact. *Circ Res*. **84**, 298–305 (1999).
35. Noden, D. M. Embryonic origins and assembly of blood vessels. *Am Rev Respir Dis*. **140**, 1097–1103 (1989).
36. Hackett, J. Jr. *et al.* Recombinant mouse-human chimeric antibodies as calibrators in immunoassays that measure antibodies to *Toxoplasma gondii*. *J Clin Microbiol*. **36**, 1277–1284 (1998).
37. Kashmiri, S. V., De Pascalis, R., Gonzales, N. R. & Schlom, J. SDR grafting—a new approach to antibody humanization. *Methods*. **36**, 25–34 (2005).
38. Morea, V., Lesk, A. M. & Tramontano, A. Antibody Modeling: Implications for Engineering and Design. *Methods*. **20**, 267–279 (2000).
39. Summa, C. M. & Levitt, M. Near-native structure refinement using in vacuo energy minimization. *Proc Natl Acad Sci USA*. **104**, 3177–3182 (2007).

## Acknowledgements

This work was supported by funds from the National Natural Science Foundation of China (NSFC81102364, NSFC81273425 and NSFC81473125), the Natural Science Foundation of Jiangsu Province (BK20140675), the Fundamental Research Funds for the Central Universities (JKY2011025), the Project Program of State Key Laboratory of Natural Medicines (China Pharmaceutical University, JKG201101) and a project funded by the Priority Academic Program Development of Jiangsu Higher Education Institutions.

## Author Contributions

X.J. and W.W. performed the experiments and wrote the main manuscript text. S.W. helped to perform the experiments. T.W. and Z.X. gave advice on experiment design. M. Wang and M. Wu supervised this study.

## Additional Information

**Supplementary information** accompanies this paper at <http://www.nature.com/srep>

**Competing financial interests:** The authors declare no competing financial interests.

**How to cite this article:** Jia, X. *et al.* A humanized anti-DLL4 antibody promotes dysfunctional angiogenesis and inhibits breast tumor growth. *Sci. Rep.* **6**, 27985; doi: 10.1038/srep27985 (2016).



This work is licensed under a Creative Commons Attribution 4.0 International License. The images or other third party material in this article are included in the article's Creative Commons license, unless indicated otherwise in the credit line; if the material is not included under the Creative Commons license, users will need to obtain permission from the license holder to reproduce the material. To view a copy of this license, visit <http://creativecommons.org/licenses/by/4.0/>